Available online at www.sciencedirect.com
ScienceDirect
International Journal of Thermal Sciences 47 (2008) 680–694
International Journal of Thermal Sciences
www.elsevier.com/locate/ijts

On large scale forest fires propagation models

O. Séro-Guillaume [a,*], S. Ramezani [a], J. Margerit [c], D. Calogine [b]

[a] *LEMTA, 2, Avenue de la Forêt de Haye, 54504 Vandoeuvre, France*
[b] *Université de La Réunion, Laboratoire Génie Industriel – EGCTH 15, Avenue René Cassin St Clotilde, 97490 Saint-Denis, France*
[c] *Université de Liège, Institut de Physique B5a, Allée du 6 Août 17, B-4000 Liège, Belgium*

Received 11 January 2007; received in revised form 7 May 2007; accepted 17 June 2007

Available online 1 August 2007

Abstract

The question of the modeling of forest fires at large scales is addressed. Empirical models are compared and it is shown that Rothermel's model describing the rate of spread of a straight front is included in the envelope model which in turn is included in a Hamilton–Jacobi equation description. This result shows that the preceding models could be included in reaction diffusion systems. Then an anisotropic propagation model with a nonlocal radiative term, obtained by asymptotic expansion of a combustion modeling, is proposed. This modeling takes into account the effects of wind and slope and it is shown that this type of modeling is the simplest generalization of the empirical ones.

Keywords: Forest fires; Envelope model; Rothermel model; Hamilton–Jacobi equation; Reaction–diffusion model

1. Introduction

Ignition and propagation of forest fires are complex phenomena involving several scales whose ranges go from micrometer to several kilometres. Actually, a unique model aiming at describing the fire at all the involved scales is probably not relevant for all the purposes of being a "propagation model", i.e., describing the propagation of the fire, and out of computational ability of computers for reasonable simulation time. So the existing propagation models must be classified by the scales they are supposed to describe and the corresponding purposes they are designed for. In order to precise with no ambiguity this classification, let us recall the different scales involved in the description of a forest fire. We will use the scales nomenclature of Séro-Guillaume and Margerit [1].

The smallest scale is the "microscopic scale". At this scale, the wood, which is the solid fuel, is a porous medium. It is composed of three phases: a solid phase, a liquid phase, and a gaseous phase. The main physical effects involved at this scale are the pyrolysis and the vaporization (or the drying) of the wood. The second considered scale is the so-called "mesoscopic scale". At this scale, all the elements of vegetation (needles, twigs, branches, leaves ...) and the air around them form a porous medium. There is an air flow and a wood outflow of combustible gas inside the pores. The geometry of the vegetation in the elementary cell plays a prominent part in the energy and momentum exchanges. In order to avoid geometrical complexity of description, we can consider a larger scale related to the typical size of the vegetation or height of the flames. At this scale, that we call "macroscopic scale", forest fuel is considered as a locally homogeneous medium composed of vegetal and gaseous constituents. Finally, if we consider a developed fire, the range of the fire size is several hundred meters to several kilometers. At this scale, that we could call "gigascopic scale", the fire interacts with the topography and the wind, the vegetation appears as a boundary layer, and the fire front is a one-dimensional line moving along a two-dimensional surface.

Corresponding to the different scales cited above, we can consider different types of models. At microscopic level, i.e., inside the solid fuel, the flow is driven by Darcy's law. A model at this scale is a "thermal degradation model" for a porous fuel, see Di Blasi [2] for example for such a modelling. The mesoscopic scale is not a relevant scale for obtaining a propagation model, because the corresponding model contains the thermal

* Corresponding author.
E-mail address: olivier.sero-guillaume@ensem.inpl-nancy.fr (O. Séro-Guillaume).

1290-0729/$ – see front matter © 2007 Published by Elsevier Masson SAS.
doi:10.1016/j.ijthermalsci.2007.06.016

degradation model cited above for the solid fuel and the usual balance equations for reactive media for the gaseous phase. This mesoscopic model can nevertheless be upscaled in order to obtain, at macroscopic scale, the combustion equations of an equivalent homogenised medium. One can speak of a "combustion model" at this scale. Such an upscaling has been derived by thermodynamics arguments in [1], and the same type of equations was given previously in Grishin [3] and Linn [4]. The pioneering works in this direction were achieved by Albini [5, 6], a combustion model and interesting 2D simulations are provided in Porterie et al. [7]. The simulations of the propagation of a developed fire of 1 km fire front length, with such a model, require the solving of the balance equations for mass, momentum, and energy for both gas and fuel phases and of the radiative transfer equation on a grid of $1000 \times 1000 \times 50 = 50 \times 10^6$ cells (of typical size 1 m) at least, which is computationally cumbersome. It is then necessary to derive, eventually from the above combustion model, a simplified model that is a "propagation model" per se, i.e., a model that is supposed to give the fire line position for real time uses.

A premixed combustion model, where, within the context of ZFK model (Majda [8]), the combustion equations reduced to a reaction diffusion system, with one equation for the energy balance and one equation for the mass fraction of fuel, is an example of a possible simplified model. The three-dimensional energy equation in the temperature T has the following form:

$$\frac{\partial T}{\partial t} + \mathbf{v}(\mathbf{x}, t) \cdot \nabla T = \varepsilon \kappa \Delta T + \varepsilon^{-1} f(T) \tag{1}$$

with $\mathbf{v}(\mathbf{x}, t)$ the gas velocity at position $\mathbf{x}$ and time t, κ the thermal diffusivity, $f(T)$ the heat source coming from the fuel combustion, and $\varepsilon = l_F/L$ is the ratio of the flame front thickness to the typical length scale of the air velocity fields. In Eq. (1), the fuel mass fraction is assumed to be constant and the velocity field $\mathbf{v}$ is assumed to be known for the sake of simplicity.

Finally, as the relevant scale for the study of forest fire propagation is the gigascopic scale, if one considers that the length scale L, involved in Eq. (1), can be assimilated to the gigascopic scale, ε could be a small parameter. Several works have been devoted to the study of the asymptotic behaviour of the system associated to (1) in the limit $\varepsilon \to 0$, see Majda and Souganidis [8], Clavin and Williams [9], for a comprehensive study. One possible leading order equation for such a simplified "flame front model" is the two-dimensional Hamilton–Jacobi equation

$$\frac{\partial G}{\partial t} + \mathbf{v}(\mathbf{x}, t) \cdot \nabla G = S_L \|\nabla G\| \tag{2}$$

In Eq. (2), the level set $G = 0$ defines the flame front position and S_L is the flame front rate of spread.

Several questions naturally arise: is it necessary to describe the forest fire propagation by a complete modelling at macroscopic level or can a reduced reaction diffusion model, at macroscopic scale, like (1) captures all the needed features of a forest fire propagation considered at large scale? Moreover, is Eq. (2), at gigascopic scale, sufficient for describing the fire propagation? The aim of this paper is to check and compare the different types of existing forest fires propagation models and to complete the previous study of Weber [10,11], attempting to give a partial answer to the two questions settled above. The approach will be the following, we will firstly present the geometrical/empirical models of Rothermel and Drouet and we will show that the latter "contains" the other. We will show then that the Drouet model or envelope model relies on a Hamilton–Jacobi equation similar to Eq. (2). And then we will see that the "simplest" extension of envelope model compatible with the Hamilton–Jacobi equation is a reaction–diffusion system.

As just mentioned before different types of models will be discussed below, but only "continuous models" will be considered. Then a special attention must be paid to cellular automata models, cf. Albinet et al. [12], Beer [13], and Weimar and Boon [14] for a complete description of these models and more recently Zekri et al. [15]. The cellular automata models consist in modelling the forest as a set of nodes on generally square lattice. The nodes can be in three states unburnt, burning or burnt. A probabilistic transition law involving the state of the node and the state of the neighbouring nodes governs the evolution of the automata. With these kinds of models, which have simple rules, and give fast computation, one can introduce the interesting concept of percolation. Above a critical density the fire propagates to infinity, whereas, under this value, the fire will extinguished. The critical density is an index of danger, which is a very useful information.

The paper is organised as follows: the second section is devoted to the description of the so-called "empirical models", namely Rothermel and envelope models. It is shown that these models are included in a Hamilton–Jacobi equation, so that they belong to gigascopic scale models. The underlying possible physical systems of partial differential equations are then evocated. The third section is dedicated to the presentation of a simplified anisotropic propagation model with a nonlocal radiative term obtained from a combustion model at macroscopic scale. In the fourth section, the comparison between this model and the envelope model is made numerically. Finally, conclusions are drawn in section five.

2. Description of the empirical models

2.1. Rothermel and envelope models

Let us recall briefly the different types of empirical model.

The Rothermel model, see Rothermel [16], relies mainly on the concept of rate of spread R that is the normal velocity of a straight fire front. If the fire front position is known at time t, the position of a point of the fire front curve that was at position $\mathbf{X}$ at time t is $\mathbf{X} + R\mathbf{n}\,\mathrm{d}t$ at time $t + \mathrm{d}t$, where $\mathbf{n}$ is the unit normal vector to the curve. The rate of spread is determined experimentally and can be expressed as a function of the local physical parameters. This function is obtained considering three relations. The first one relates the link between the so-called total propagating heat flux I_p and the rate of spread

$$R = \frac{I_p}{\rho_{be} Q_{ig}} \tag{3}$$

where Q_{ib} is the heat required to ignite a unit mass of fuel and ρ_{be} is the effective bulk density, i.e., the amount of fuel per unit

volume of the fuel bed raised to ignition ahead of the advancing fire. The second relation is the experimental correlation

$$I_{p0} = I_{p0}(I_R) \tag{4}$$

between the total propagating heat flux I_{p0}, without wind and slope, and the reaction intensity I_R which is the product of the fuel mass loss rate per unit area and the fuel heat content H:

$$I_R = -\frac{\mathrm{d}m}{\mathrm{d}t} H \tag{5}$$

The last relation is an empirical relation that takes into account the role of wind and slope. It is indeed assumed that the influence of wind and slope can be handled by two parameters which have to be measured experimentally. This relation gives the total propagating heat flux I_p as a function of the same flux I_{p0} without wind and slope and has the following form:

$$I_p = I_{p0}(1 + \phi_w + \phi_s) \tag{6}$$

where ϕ_w and ϕ_s are respectively wind and slope correlation factors, and are function of the local physical parameters. Once the empirical relations (4)–(6) are inserted in (3), one obtain the relation

$$R = R(\sigma, \delta, C_0, \rho_p, H, V, \tan\varphi, M_f, M_x, S_T, S_E) \tag{7}$$

where the local physical parameters are given in Table 1.

Let us now go to the so-called envelope models. It is experimentally known, see Peet [17] for example, that a fire ignited at a point in a uniform forest under the action of wind or slope can develop as a curve like an ellipse with the great axis aligned with wind or slope, see Fig. 1. The equations of the ellipse can be written:

$$\begin{cases} \tilde{X}(t,\phi) = t(g + f\cos\phi) \\ \tilde{Y}(t,\phi) = th\sin\phi \end{cases} \tag{8}$$

The parameters f, g, and h are homogeneous to a velocity and must be determined experimentally.

Relying on this experimental evidence, independently Drouet [18] and Anderson et al. [19] have developed the so-called envelope model that is valid for a nonuniform forest. Within this description, parameters f, g, and h depend now on time t, position $\mathbf{X}$, and wind or slope direction $\mathbf{k}$, because they depend on local physical properties of the forest (as fuel moisture, heat diffusivities, ...), on hydrodynamics of the gas, and on slope. Between time t and $t + \mathrm{d}t$, all points of the fire front are source points and the fire front at time $t + \mathrm{d}t$ is the envelope of all these ellipses. Once the parameters have been fitted, this model produces realistic scenarios of propagation, see Catchpole et al. [20]. Richards [21] has derived a set of analytical equations for obtaining directly the position of the fire front. To get these equations, let us denote the local unit vector giving the local direction of the wind or of the slope by $\mathbf{k}(M,t) = \mathbf{i}\cos(\beta(t)) + \mathbf{j}\sin(\beta(M,t))$, and $\mathbf{k}^{\perp}(M,t)$ its orthogonal vector (cf. Fig. 2).

Here $(\mathbf{i},\mathbf{j})$ is a global basis. The fire front is the curve denoted by C_t, parameterised by θ, and let $\mathbf{X}(t,\theta) = X(t,\theta)\mathbf{i} + Y(t,\theta)\mathbf{j}$ be the position vector describing this fire front curve. It can be shown, using the theory of envelopes, see Richards [21],

Table 1
Meaning of local physical parameters involved in relation (7)

σ	Surface-area-to-volume ratio of fuel elements (m^{-1})
δ	Vegetal layer depth (m)
C_0	Fuel load ($\mathrm{kg\,m}^{-2}$)
ρ_p	Density of dry particles ($\mathrm{kg\,m}^{-3}$)
H	Fuel heat content ($\mathrm{kJ\,kg}^{-1}$)
V	Wind velocity ($\mathrm{m\,s}^{-1}$)
$\tan\varphi$	Slope
M_f	Humidity of fuel particles
M_x	Extinction humidity
S_T	Mass fraction of total minerals in fuel particles
S_E	Mass fraction of minerals without silica in fuel particles

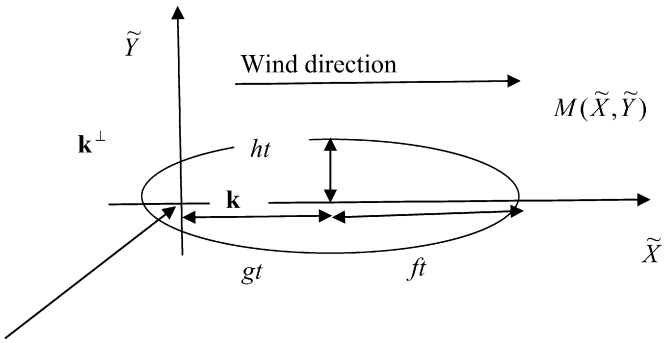

Fig. 1. Propagation of a point ignited fire.

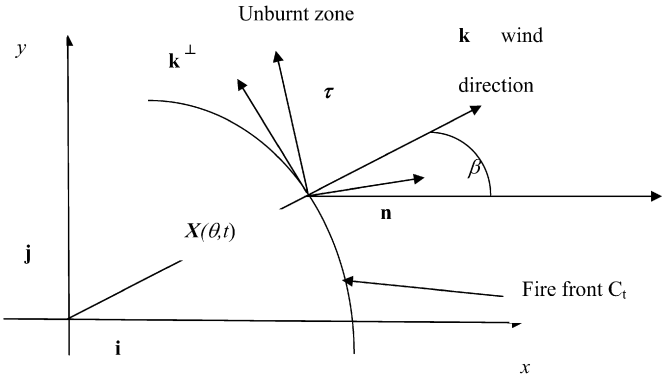

Fig. 2. Fire front description.

that the system of partial differential equations (PDE) that the co-ordinates of a point on the fire front has to verify is

$$\begin{cases} \frac{\partial X}{\partial t}(\theta,t) = g(\mathbf{X},t,\beta)\cos(\beta) + r[pf(\mathbf{X},t,\beta)^2\cos(\beta(\mathbf{X},t)) \\ \quad + qh(\mathbf{X},t,\beta)^2\sin(\beta(\mathbf{X},t))] \\ \frac{\partial Y}{\partial t}(\theta,t) = g(\mathbf{X},t,\beta)\sin(\beta) + r[pf(\mathbf{X},t,\beta)^2\sin(\beta(\mathbf{X},t)) \\ \quad - qh(\mathbf{X},t,\beta)^2\cos(\beta(\mathbf{X},t))] \end{cases} \tag{9}$$

where the functions p, q, and r are given by

$$\begin{cases} p(\theta,t) = -\frac{\partial X}{\partial\theta}\sin(\beta(\mathbf{X},t)) + \frac{\partial Y}{\partial\theta}\cos(\beta(\mathbf{X},t)) \\ q(\theta,t) = \frac{\partial X}{\partial\theta}\cos(\beta(\mathbf{X},t)) + \frac{\partial Y}{\partial\theta}\sin(\beta(\mathbf{X},t)) \\ r(\theta,t) = [(f(\mathbf{X},t,\beta)p(\theta,t))^2 + (h(\mathbf{X},t,\beta)q(\theta,t))^2]^{-1/2} \end{cases} \tag{10}$$

Eqs. (9) and (10) form a system of nonlinear PDE that must be solved for determining the fire front position. Note that, for the particular case of a uniform forest with uniform wind and slope, we can take $(\mathbf{i},\mathbf{j}) = (\mathbf{k},\mathbf{k}^{\perp})$ so that $\beta = 0$ and Eqs. (9)–(10) are simplified. It is then straightforward to verify that Eq. (8) is solution to Eqs. (9)–(10). That proves the coherence of the envelope method.

In order to compare this approach with the point of view of Rothermel, let us determine the rate of spread, i.e., the normal velocity $\dot{\mathbf{X}}\cdot\mathbf{n}$ of the fire front, where we denote by $\boldsymbol{\tau}$ and $\mathbf{n}$ the unitary tangent and normal vectors to C_t and $\dot{\mathbf{X}} = \frac{\partial \mathbf{X}}{\partial t}$. As

$$\frac{\partial \mathbf{X}}{\partial \theta} = \rho\boldsymbol{\tau}, \quad \text{with } \rho = \left\| \frac{\partial \mathbf{X}}{\partial \theta} \right\|$$

by definition of $\boldsymbol{\tau}$, using the vectors $\mathbf{k}$ and $\mathbf{k}^{\perp}$, relation (9) can be written in the intrinsic form

$$\dot{\mathbf{X}} = \left[\big(g(\mathbf{X},t,\mathbf{k}) + f(\mathbf{X},t,\mathbf{k})^2\bar{r}\bar{p}\big)\mathbf{k} - h(\mathbf{X},t,\mathbf{k})^2\bar{r}\bar{q}\mathbf{k}^{\perp}\right] \tag{11}$$

with

$$\begin{cases} \bar{p}(\theta,t) = \mathbf{k}\cdot\mathbf{n} \\ \bar{q}(\theta,t) = \mathbf{k}\cdot\boldsymbol{\tau} = -\mathbf{k}^{\perp}\cdot\mathbf{n} \\ \bar{r}(\theta,t) = [(f(\mathbf{X},t,\mathbf{k})\bar{p})^2 + (h(\mathbf{X},t,\mathbf{k})\bar{q})^2]^{-1/2} \end{cases} \tag{12}$$

so that the normal velocity of the fire front takes the simple form

$$\dot{\mathbf{X}}\cdot\mathbf{n} = g(\mathbf{X},t,\mathbf{k})\bar{p} + \left[\big(f(\mathbf{X},t,\mathbf{k})\bar{p}\big)^2 + \big(h(\mathbf{X},t,\mathbf{k})\bar{q}\big)^2\right]^{1/2} \tag{13}$$

We can define the following tensor

$$\mathbf{C}(M,t,\mathbf{k}) = \begin{pmatrix} f(M,t,\mathbf{k}) & 0 \\ 0 & h(M,t,\mathbf{k}) \end{pmatrix}_{(\mathbf{n},\boldsymbol{\tau})} \tag{14}$$

so that Eq. (13) takes finally the compact form

$$\dot{\mathbf{X}}\cdot\mathbf{n} = g(\mathbf{X},t,\mathbf{k})\mathbf{k}(\mathbf{X},t)\cdot\mathbf{n} + \big\|\mathbf{C}(\mathbf{X},t,\mathbf{k})\cdot\mathbf{k}(\mathbf{X},t)\big\| \tag{15}$$

Now, if we consider a straight front that propagates in a uniform forest, $\mathbf{n} = \mathbf{k}$ so that relation (15) reduces to $\dot{\mathbf{X}}\cdot\mathbf{n} = g(\mathbf{X},t,\mathbf{k}) + f(\mathbf{X},t,\mathbf{k})$. This proves that the empirical rate of spread R given by Eq. (7) and empirical parameters g and f are linked by the relation

$$R = g + f \tag{16}$$

The Rothermel model is then structurally include in the envelope method.

2.2. Envelope model and Hamilton–Jacobi equation

We will demonstrate now that envelope model is included in a Hamilton–Jacobi equation. The link between these two approaches is the Huygens principle. For chemical waves in reactive systems the Huygens principle can indeed be applied, see Sieniutycz and Farkas [22] or Enders [23] for a general description and we will apply it to forest fires. We can imagine the propagation of the fire as the propagation of an interaction in an excited medium. The propagation takes place with the following rules:

(i) Every point of the medium can be excited or not (the point is burning or not).

(ii) Once a point is excited, it becomes the source of an excitation.

We can consider that the velocity $c(\mathbf{x},\mathbf{x}')$ of the propagation of the excitation in the direction $\mathbf{x}'$ at a point $P(\mathbf{x})$ is given by

$$c(\mathbf{x},\mathbf{x}') = \frac{1}{F(\mathbf{x},\mathbf{x}')}\|\mathbf{x}'\| \tag{17}$$

where the indicatrix function $F(\mathbf{x},\mathbf{x}')$ must satisfy the three following properties:

(i) $F(\mathbf{x},\mathbf{x}') > 0$ if $\mathbf{x}' \neq 0$. (18)

(ii) It is a positively homogeneous function of the direction, because the velocity does not depend on the parameterisation of the paths, i.e.,

$$F(\mathbf{x},\lambda\mathbf{x}') = \lambda F(\mathbf{x},\mathbf{x}'), \quad \forall\lambda \neq 0 \tag{19}$$

(iii) We suppose that $F(\mathbf{x},\mathbf{x}')$ is a smooth function of $\mathbf{x}$.

Let us consider an excited point P_0. The time taken by the perturbation to go to another point P_1 at rest, on the path $\tilde{\gamma}$ is $\tau(P_0,P_1,\tilde{\gamma}) = \int_{\mathbf{x_0}}^{\mathbf{x}_1} F(\mathbf{x}(\tilde{\gamma},s), \frac{\mathrm{d}\mathbf{x}}{\mathrm{d}s}(\tilde{\gamma},s))\,\mathrm{d}s$ where s is the arc length along the path and $\mathbf{x}(\tilde{\gamma},s)$ is the position vector describing the path $\tilde{\gamma}$. As the point P_1 will become excited once the first perturbation has reached it, the real path of the perturbation will be the one for which the time τ is the minimum, that is

$$\tau(P_0,P_1) = \min_{\tilde{\gamma}} \tau(P_0,P_1,\tilde{\gamma}) \tag{20}$$

If the excited domain at time t_0 is $D_e(t_0)$, the real time for the perturbation to attain P_1 is

$$\tau(P_1) = \min_{P_0\in D_e(t_0)} \tau(P_0,P_1) \tag{21}$$

This is this Huygens principle that describes the position of the fire front perturbation.

In order to determine the indicatrix function $F(\mathbf{x},\mathbf{x}')$ related to the envelope model, let us consider the ellipse due to the source point P_0. In the local system of co-ordinates $(\tilde{X},\tilde{Y})$, see Fig. 1 for notations, the equations for this ellipse are

$$\begin{cases} \tilde{X}(\phi,\mathrm{d}t) = \mathrm{d}t[g(P_0,t_0) + f(P_0,t_0)\cos\phi] \\ \tilde{Y}(\phi,\mathrm{d}t) = \mathrm{d}t[h(P_0,t_0)\sin\phi] \end{cases} \tag{22}$$

Eliminating the parameter angle ϕ, we obtain the equation

$$G\left(\frac{\tilde{X}}{\mathrm{d}t},\frac{\tilde{Y}}{\mathrm{d}t}\right) = 1 \tag{23}$$

with

$$G(x_1',x_2') = \frac{1}{f^2}(x_1' - g)^2 + \frac{1}{h^2}x_2'^2 \tag{24}$$

The point which is attained after time $\mathrm{d}t$, in the direction of the unitary vector $\mathbf{x}' = (x_1',x_2')$, where $x_1' = \mathbf{x}'\cdot\mathbf{k}$ and $x_2' = \mathbf{x}'\cdot\mathbf{k}^{\perp}$, has the co-ordinates $\tilde{X} = c(\mathbf{x},\mathbf{x}')x_1'\,\mathrm{d}t$ and $\tilde{Y} = c(\mathbf{x},\mathbf{x}')x_2'\,\mathrm{d}t$, so that the velocity $c(\mathbf{x},\mathbf{x}')$ satisfies the equation $G(cx_1',cx_2') = 1$. As $F(\mathbf{x},\mathbf{x}') = \frac{1}{c}$, the indicatrix function is solution to the equation

$$G\left(\frac{x_1'}{F},\frac{x_2'}{F}\right) = 1 \tag{25}$$

whose appropriated solution is

$$F(\mathbf{x},\mathbf{x}') = \frac{-B-\sqrt{B^2-AC}}{C} \tag{26}$$

where

$$\begin{cases} A = \frac{1}{h^2}[(h/f)^2(\mathbf{x}'\cdot\mathbf{k})^2 + (\mathbf{x}'\cdot\mathbf{k}^{\perp})^2] \\ B = -\frac{h}{f}(g/f)(\mathbf{x}'\cdot\mathbf{k})\frac{1}{h} \\ C = (g/f)^2 - 1 \end{cases} \tag{27}$$

Let us now consider the function $S(\mathbf{x},t)$ defined by

$$S(\mathbf{x},t) = -t + \tau(\mathbf{x}) \tag{28}$$

where τ is the minimum time considered in (21). The position of the fire front is given by the relation

$$S(\mathbf{x},t) = 0 \tag{29}$$

The function S is solution to the following Hamilton–Jacobi equation, see Courant and Hilbert [24],

$$\frac{\partial S}{\partial t} + H(\mathbf{x},\nabla S) = 0 \tag{30}$$

where the function H is the Hamiltonian, defined by the following Legendre transformation:

$$H(\mathbf{x},\mathbf{p}) = \sup_{\mathbf{x}'} \frac{\langle \mathbf{p},\mathbf{x}'\rangle}{\|\mathbf{x}'\|_F} \tag{31}$$

with $\langle .,.\rangle$ the usual scalar product and $\|\mathbf{x}'\|_F = F(\mathbf{x},\mathbf{x}')$.

After some algebra one can find from relations (31) and (26):

$$H(\mathbf{x},p_1,p_2) = gp_1 + \sqrt{(fp_1)^2 + (hp_2)^2} \tag{32}$$

which is nothing but right-hand size of relation (13), the normal velocity of the front. This result can indeed be derived directly from the Hamilton–Jacobi equation. The normal velocity of the curve defined by (29) is indeed $\dot{\mathbf{X}}\cdot\mathbf{n} = -\frac{1}{\|\nabla S\|}\frac{\partial S}{\partial t}$, so that using the Hamilton–Jacobi equation (30), we get

$$\dot{\mathbf{X}}\cdot\mathbf{n} = \frac{H(\mathbf{x},\nabla(S))}{\|\nabla S\|} \tag{33}$$

Let us recall that $\bar{p}$ and $\bar{q}$ are components of the direction of the wind on the tangent and normal basis of the curve given by (12), so that $\frac{\partial S}{\partial x_1} = \bar{p}\|\nabla S\|$ and $\frac{\partial S}{\partial x_2} = \bar{q}\|\nabla S\|$. Finally, we obtain the following rate of spread:

$$\dot{\mathbf{X}}\cdot\mathbf{n} = \frac{H(\mathbf{x},\bar{p}\|\nabla S\|,\bar{q}\|\nabla S\|)}{\|\nabla S\|} = H(\mathbf{x},\bar{p},\bar{q}) \tag{34}$$

because the Hamiltonian is an homogeneous function of order one in $\mathbf{p} = (\bar{p},\bar{q})$.

We can conclude that the envelope model is structurally included in Hamiltonian modelling, the envelope method being only a way of solving the Hamilton–Jacobi equation. Note that Hamilton–Jacobi equation (30) can leads to nonelliptical fire propagation if we choose another Hamiltonian than the one given by Eq. (32).

All above empirical models fall, in fact, within the context of a geometrical description of the fire front, so that they should be called "empirical/geometrical models" rather than empirical models. We have obtained so far a pure geometrical model, with no a priori relations with any physical process. Once the parameter functions are adjusted, the simulations made with this model give relatively realistic shapes for the fire front, see Finney [25]. We will see that the link between this approach and a physical model can be made via the use of the Hamilton–Jacobi equation (30). In the particular case when $f = h$, then Eq. (30) reduced indeed to

$$S_t + g\mathbf{k}\cdot\nabla S = f\|\nabla S\| \tag{35}$$

We recover the G equation (2) for a flame front in premixed flame with $\mathbf{v} = g\,\mathbf{k}$ and $S_L = f$. This suggests that models considered in this section are descriptions of the fire front at very large scale (gigascopic) and that the leading underlying physical process is a reaction diffusion system. We will precise this point in the following Section 2.3.

2.3. Possible relationship of the envelope model with physical equations

The models considered in the previous section are very attractive because they are two dimensional models that depends only on three parameters, namely f, g, and h, and they give very fast computations. These parameters have to be estimated as functions of physical measurable parameters from real experiments or eventually numerical experiments. When these parameters are well chosen, the simulated propagations of the fire front are realistic for many usual situations. Several questions remain:

1. What are the main underlying physical processes leading to Hamilton–Jacobi equation (30)?
2. What is the range of validity of the geometrical/empirical models described above?

The fire front can indeed be assimilated to a characteristic surface, say $T = \text{cst}$, of a system of PDE, where the variable T is a temperature and the constant could be an ignition temperature. It has been indeed shown in [11] that the level curves of the equation

$$\frac{\partial T}{\partial t} + \mathbf{A}(\mathbf{x})\cdot\nabla T = \nabla\cdot\big(\big(\mathbf{C}^2(\mathbf{x})/W(\mathbf{x})\big)\nabla T\big) + W(\mathbf{x})T \tag{36}$$

with

$$\mathbf{A}(\mathbf{x}) = \begin{pmatrix} g \\ 0 \end{pmatrix}, \qquad \mathbf{C}(\mathbf{x}) = \begin{pmatrix} f(\mathbf{x}) & 0 \\ 0 & h(\mathbf{x}) \end{pmatrix} \tag{37}$$

and $W(\mathbf{x})$ a known reaction source function, can develop as ellipses from a Dirac point source, provided that the above coefficients are constant. Therefore, reaction–diffusion systems are good candidates as underlying processes for the propagation of forest fires at large scale.

It is known however, cf. Courant and Hilbert [24], that the solution of characteristic surfaces of hyperbolic systems of equations, satisfies a Hamilton–Jacobi equation too, so that the underlying physical process could be hyperbolic too. One can see indeed, cf. [24], that the solutions of the Hamiltonian equation (30) with Hamiltonian given by relation (32) are, in the case $g = 0$, characteristic curves of the equation

$$\frac{\partial^2 T}{\partial t^2} + \frac{1}{\tau}\frac{\partial T}{\partial t} = \nabla\cdot(\mathbf{C}^2\nabla T), \quad \text{with } \mathbf{C} = \begin{pmatrix} f(\mathbf{x}) & 0 \\ 0 & h(\mathbf{x}) \end{pmatrix} \tag{38}$$

In Eq. (38), the functions f and h are the one involved in the model of propagation and τ is an unknown relaxation time.

The question now is the status of the "temperature" T in (36) or/and (38). In general three dimensional combustion models cited previously, the forest is considered as a stratified medium. Above the vegetation, the equations for the model are the one of a multi-constituents gaseous phase with chemical reactions and radiation heat transfer, and the vegetation has been homogenised at macroscopic scale and is considered as a porous multiphasic multi-components medium, i.e. the forest fuel is a complex medium with two phases at least, namely the solid vegetation phase and the fluid phase, composed of air and of gases issued from the vegetation pyrolysis. Then there are two temperatures, namely T_p for the solid phase and T_f for the gaseous phase. And the question is to know what temperature has to be considered in models based on Eq. (36) or (38). And it is often argued that the equivalent or homogenised medium is not at thermal equilibrium so that the temperature equations for the solid and fluid phase are not the same. Then it is nevertheless tempting to assume at first approximation that the thermal equilibrium is reached in forest layer, i.e., $T_p = T_f$, so that, one can show, [1], that the energy balance reduces to

$$\begin{aligned}&\left(\Phi\rho_f C_P^f + (1-\Phi)\rho_p C_P^p\right)\frac{\partial T}{\partial t} + \Phi\rho_f C_P^f \mathbf{V}_f\cdot\nabla T \\ &\quad + \nabla\cdot(\lambda\nabla T + \mathbf{Q}_r) = R_{fc} + R_{pc}\end{aligned} \tag{39}$$

where $T = T_p$, Φ is the porosity of the porous forest medium, ρ_f and C_P^f are the density and heat capacity of the fluid phase, ρ_p and C_P^p are the density and heat capacity of the solid porous phase, $\mathbf{Q}_r$ is the radiative flux, and R_{fc} and R_{pc} are the heat sources due to chemical reactions in both phases. Finally, $\mathbf{V}_f$ is the velocity of the gas and λ the equivalent conductivity. This result is in accordance with the study of Moyne et al. [26] on the modelling of heat transfer in porous media. This equation (39) looks like the reaction–diffusion equation (36). The discrepancy between both equations is the isotropy of the conductivity and the presence of a radiative flux $\mathbf{Q}_r$ in Eq. (39). Note that if the forest medium is dense enough the radiative term can reduces to a diffusion one.

The use of Eq. (39) for simulating forest fires propagation supposes the knowledge of the velocity $\mathbf{V}_f$ of the gas, and then requires the solving of the related Navier–Stokes equation inside the vegetal phase. But, one can realise that the convective term $(\Phi\rho_f C_P^f \mathbf{V}_f\cdot\nabla T)$ in (39) can be neglected inside the vegetation, for two reasons. The first one is that density of gases is largely smaller than the one of solid phase and that the velocity of gases is in the range of only some meters per second. The second reason is that the Reynolds number is at least of 10^5 and the flow is turbulent (let us recall that $\Phi \approx 0.9$), then once it is averaged in time the convective term $(\Phi\rho_f C_P^f \mathbf{V}_f\cdot\nabla T)$ contributes to diffusion more than to convection, see for example the paper by Fannjiang and Papanicolaou [27]. At the end of this section we are in position to assert that the temperature of the solid phase is the relevant parameter for describing the propagation. However, as we will see in the next section, it is important to deal with the developed flames above the vegetation when we consider the reduction to two-dimensional propagation model. The role of the velocity of the gas above the vegetation is important because it influences the direction of the flame and then radiation.

3. Physical system for forest fires propagation

The system of reaction diffusion equations dedicated to the simulation of forest fires propagation could be set "a priori" cf. Weber [10] or derived from a system of equations describing the fires at smaller scale, i.e., at macroscopic scale. In this section, for sake of completeness we will recall, see [28], the derivation of this system.

3.1. A two-dimensional reaction diffusion system for forest fire propagation

The detailed combustion model, from which the propagation model is derived is the one developed in [1], and we refer to this paper for the details of notations and derivations. Let us recall some notations introduced in the preceding section. The forest is considered as a porous medium of porosity Φ, composed of a vegetal phase with index p and a fluid gaseous phase with index f. The vegetal phase is itself composed of different constituents; for sake of simplicity only water (liquid or gaseous), cellulose, char, and flammable gas due to pyrolysis, are considered; T_p is the temperature of the vegetal phase and T_f is the temperature of the gaseous phase.

Let us consider that the mean height scale of the vegetal stratum is δ, and we suppose that the height of flame is of the same magnitude. We can consider now a gigascopic scale L associated to a developed fire or corresponding to a distance from the flames front such that the ratio $\varepsilon = \delta/L$ is a small parameter, say $\varepsilon \ll 1$. At scale L, the vegetation appears as a boundary layer and the fire can be considered as spreading on a surface. We consider an asymptotic expansion with ε as small parameter in order to derive the model, which corresponds to the inner expansion, in the sense of matched asymptotic expansion. The obtained model is complex but we retain only the part corresponding to the energy and mass balances equations of the vegetal:

$$\begin{aligned}(1-\Phi)\rho_p C_P^p\frac{\partial T_p}{\partial t} &= \nabla_S\cdot(\lambda_p\nabla_S T_p) \\ &\quad - \nabla_S\cdot\mathbf{Q}_{rp} + R_{cp} + \chi(T_f - T_p) + M_r\end{aligned} \tag{40}$$

$$\begin{aligned}&\frac{\partial}{\partial t}\left((1-\Phi)(1-\varepsilon^p)Sa_{w_p}\right) \\ &\quad = -(1-\Phi)(1-\varepsilon^p)Sa_{w_p}k_{w_pc_p}(T_p)\end{aligned} \tag{41}$$

$$\begin{aligned}&\frac{\partial}{\partial t}\left((1-\Phi)(1-\varepsilon^p)Sa_{c_p}\rho_{c_p}\right) \\ &\quad = (1-\Phi)(1-\varepsilon^p)Sa_{w_p}\rho_{w_p}k_{w_pc_p}(T_p)\end{aligned} \tag{42}$$

$$\begin{aligned}&\frac{\partial}{\partial t}\left((1-\Phi)\varepsilon^p Sa_{l_p}\right) \\ &\quad = -(1-\Phi)\varepsilon^p Sa_{l_p}k_{l_pv_{gp}}(T_p)\end{aligned} \tag{43}$$

with

$$C_P^p = (1-\varepsilon^p)\left(Sa_{w_p}\frac{\rho_{w_p}}{\rho_p}C_{P_{w_p}} + Sa_{c_p}\frac{\rho_{c_p}}{\rho_p}C_{P_{c_p}}\right) + \varepsilon^p\left(Sa_{l_p}\frac{\rho_{l_p}}{\rho_p}C_{P_{l_p}}\right)$$

and the heat source R_{cp} a known function of temperature T_p, ∇_S is a surfacic operator set on the surface of propagation and λ_p is the conductivity of the vegetal phase, the different terms Sa_j represent the saturation of different components of the vegetal medium, and ε^p is the proper porosity of the vegetal phase. In Eq. (40), which represents balance of energy of the solid phase, the term R_{cp} is the heat source due to evaporation and pyrolysis, the term $-\nabla_S \cdot \mathbf{Q}_{rp}$ is the heat source due to the solid phase combustion, and the term $\chi(T_f - T_p)$ is the heat flow convection term due to interaction of the vegetation with the ambient gas at temperature T_f, and M_r is the radiative heat source coming from the flames. Index w_p is for the wood constituent who is subject to pyrolysis, c_p is for char constituent of wood, while the index l_p is for the liquid phase in the wood, the terms $k_{w_p c_p}$ and $k_{l_p v_{gp}}$ are associated to the pyrolysis and drying.

All the preceding equations (40)–(43) are part of the equations of the boundary layer produces by the fire. The solution of the complete system of equations should be matched to the solution of the outer expansion, i.e., to equations above the forest fire layer, for determining the radiative heat source M_r coming from the flames and the gaseous temperature field T_f.

3.2. Derivation of a simplified two-dimensional anisotropic propagation model with nonlocal radiative term

Let us consider a simplified version of the preceding model. The first approximation that we can do is to suppose that evaporation is at constant temperature T_{ev}, which simplifies Eq. (43), and neglect the heat absorbed by solid during pyrolysis. A cruder approximation is to neglect the radiative heat transfer $-\nabla_S \cdot \mathbf{Q}_{rp}$ into the forest layer and the char residue (Eq. (42)) so that Eq. (40) reduces to

$$(1-\Phi)\rho_p(C_s + H_u C_l)\frac{\partial T}{\partial t} = \nabla\cdot(\lambda\nabla T) + h(T_a - T) + (1-\Phi)\rho_p\frac{\partial H_u}{\partial t}L_{ev}\delta_{T=T_{ev}} + M_r \quad (44)$$

In this relation, we have suppressed the indices of operators and of temperature, H_u is the humidity the symbol $\delta_{T=T_{ev}}$ stands for the Dirac distribution of the zone $T = T_{ev}$ and M_r is the total radiative flux coming from the flame. Moreover, $C_p = C_s + H_u C_l$ with C_s is the heat capacity of the solid constituent of vegetation, C_l is the heat capacity of the water, h is the heat loss coefficient, T_a is the temperature of the gaseous ambient phase, and L_{ev} is an evaporation latent heat.

Now the simplification can be summed up as follows:

(i) In the zone before the evaporation front, denoted by zone I, such that $T < T_{ev}$ and $\rho_p > \rho_{\text{ext}}$,

$$(1-\Phi)\rho_p(C_s + H_{u0}C_l)\frac{\partial T}{\partial t} = \nabla\cdot(\lambda\nabla T) + M_r - h(T - T_a) \quad (45)$$

where H_{u0} is the initial humidity and ρ_{ext} the extinction vegetation density.

(ii) In the evaporation zone, denoted by zone II, such that $T = T_{ev}$, $H_u > 0$ and $\rho_p \geqslant \rho_{\text{ext}}$,

$$-(1-\Phi)\rho_p L_{ev}\frac{\partial H_u}{\partial t} = M_r - h(T_{ev} - T_a) \quad (46)$$

(iii) In the intermediary zone between the evaporation zone and the burning zone, denoted by zone III, such that $T_{ev} < T < T_i$, $H_u = 0$ and $\rho_p \geqslant \rho_{\text{ext}}$,

$$(1-\Phi)\rho_p C_s\frac{\partial T}{\partial t} = \nabla\cdot(\lambda\nabla T) + M_r - h(T - T_a) \quad (47)$$

with T_i the ignition temperature.

(iv) In the burning zone, denoted by zone IV, such that $T \geqslant T_i$, $H_u = 0$ and $\rho_p \geqslant \rho_{\text{ext}}$,

$$(1-\Phi)\rho_p C_s\frac{\partial T}{\partial t} = \nabla\cdot(\lambda\nabla T) + M_r - h(T - T_a) \quad (48)$$

the variation of mass due to chemical reactions is:

$$\frac{\partial \rho_p}{\partial t} = -v_r\rho_p \quad (49)$$

where v_r characterizes the speed of the chemical reaction, one can consider an Arrhenius law

$$v_r = A\exp(-E/RT) \quad (50)$$

(v) In the burnt zone, denoted by zone V, such that $\rho_p = \rho_{\text{ext}}$

$$(1-\Phi)\rho_{\text{ext}}C_s\frac{\partial T}{\partial t} = \nabla\cdot(\lambda\nabla T) + M_r - h(T - T_a) \quad (51)$$

3.3. Simplified radiative flame model

As it has been noted at the end of Section 3.2, the preceding model (45)–(51) corresponds to an inner expansion while the radiative flux term M_r can only be calculated from the solution of the outer expansion. As this is not the aim of this paper to precise this expansion, and for illustration, we consider a simplified flame model that introduces nonlocal effects due to radiation.

The vegetation is supposed to be very thin and set on a plane S_f. The flame is supposed to be at constant known temperature T_f and each flame element is supposed to be directed by a unit vector $\mathbf{F}$, the emitting point is denoted by $\mathbf{P}$ and the receiving point by $\mathbf{M}$, $\mathbf{O}$ is the flame foot (cf. Fig. 3). The global basis is denoted by $(\mathbf{e}_1, \mathbf{e}_2, \mathbf{e}_3)$, $\mathbf{e}_3$ being the vertical direction. The vector $\mathbf{n}$ is the unit normal to the upper plane (i.e. unit normal to the receiving surface) of the vegetation at $\mathbf{M}$. The angle between $\mathbf{F}$ and the vertical is denoted by $\alpha_f = (\mathbf{e}_3, \mathbf{F})$. The flame elements are supposed to have a length l_f. If the fire front is supposed to be thin, one can show that the radiative heat flux is given by the double integral calculated on the burning zone denoted by S_f:

$$M_r = K_f\frac{BT_f^4}{\pi}$$

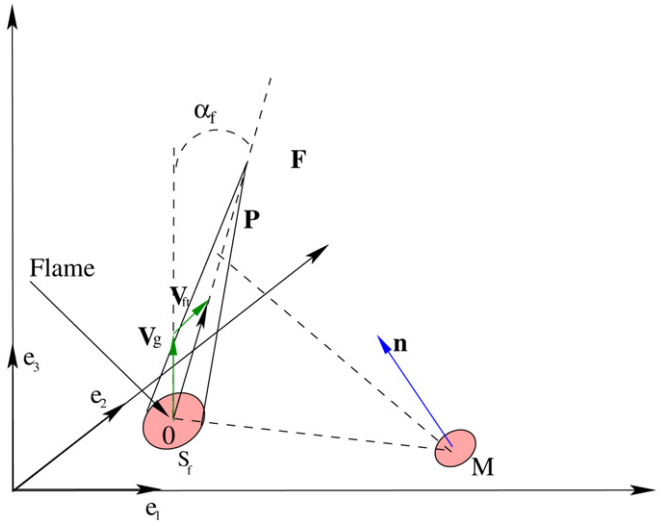

Fig. 3. Radiation of the flame.

$$\times \int_{S_f} \frac{(\mathbf{F}(1-\cos\theta_{f_m}) - \mathbf{w}(\cos\beta - \cos(\beta+\theta_{f_m}))\cdot\mathbf{n}}{r\sin^2\beta}\,\mathrm{d}x\,\mathrm{d}y \tag{52}$$

with, cf. Appendix A for notation and derivation, r being the distance between the foot flame and the receiving points, and K_f the absorption coefficient of the flame,

$$\cos\beta = \mathbf{F}\cdot\frac{\mathbf{OM}}{r} = \mathbf{F}\cdot\mathbf{w} \tag{53}$$

$\mathbf{w}$ is the unit vector such that $\mathbf{OM} = r\mathbf{w}$.

$$\cot\theta_{f_m} = -\cot\beta + \frac{r}{l_f\sin\beta} \tag{54}$$

The velocity of the gas is decomposed as follows $\mathbf{V}_{fl} = \mathbf{v}_g + \mathbf{V}$, with

$$\begin{cases} \mathbf{v}_g = V_g\mathbf{e}_3 \\ \mathbf{V} = V_g(\cos\varphi_v\mathbf{k} + \sin\varphi_v\mathbf{k}^\perp) \\ \mathbf{V}^t_{fl} = \mathbf{V}_{fl} - (\mathbf{V}_{fl}\cdot\mathbf{e}_3)\mathbf{e}_3 \end{cases} \tag{55}$$

4. Numerical comparison of models

We are now in position of comparing the anisotropic propagation model with a nonlocal radiative term, given at Sections 3.2. and 3.3. Eqs. (45)–(55), with the envelope model. We consider a uniform forest. Typically the following values have been considered for the physical parameters of the model, given in Table 2, with $A = 5\times10^3\ \mathrm{s}^{-1}$, $E = 1.398\times10^5\ \mathrm{J\,mole}^{-1}$, $\Phi = 0.9$, $\rho_{\mathrm{ext}} = 0$, and $R = 8.314\ \mathrm{J\,mole}^{-1}\,\mathrm{K}^{-1}$.

As mentioned before at the end of Section 2, the convective term through the forest gives rise to diffusion at large scale so that the equivalent heat diffusivity λ value of the forest is different from the conductivity of the vegetation. This value should then be estimated by inverse method from fire tunnel experiments or numerical sub grid simulations. The precise study of the influence of the heat diffusivity on the fire front spread is beyond the scope of this paper. Nevertheless, Chetehouna et al. [29] have shown that the rate of spread can be computed by a regular perturbation expansion in the diffusion. Then the diffusion contribution is small regarding radiative heat flux contribution so that we will consider that the heat diffusivity λ is null at first approximation. This is nevertheless the nonlocal radiative term that will play the role of anisotropic and convective terms.

The calculations of model equations (45)–(55) have been made with a finite volume method in a domain of $10\times10\ \mathrm{m}^2$, the grid mesh sizes are 0.5 m, 0.25 m, 0.1 m, and the time step is 1.0 s.

Table 2
Parameters model value

$C_s = 2400\ \mathrm{J\,kg}^{-1}\,\mathrm{K}^{-1}$	$C_l = 4180\ \mathrm{J\,kg}^{-1}\,\mathrm{K}^{-1}$
$\delta = 1$ m	$K = 0.2\ \mathrm{m}^{-1}$
$h = 20\ \mathrm{J\,m}^{-2}\,\mathrm{s}^{-1}\,\mathrm{K}^{-1}$	$L_{ev} = 2.250\times10^6\ \mathrm{J\,kg}^{-1}$
$T_a = 300$ K	$T_{ev} = 373$ K
$h_f = 1$ m	$T_f = 1200$ K

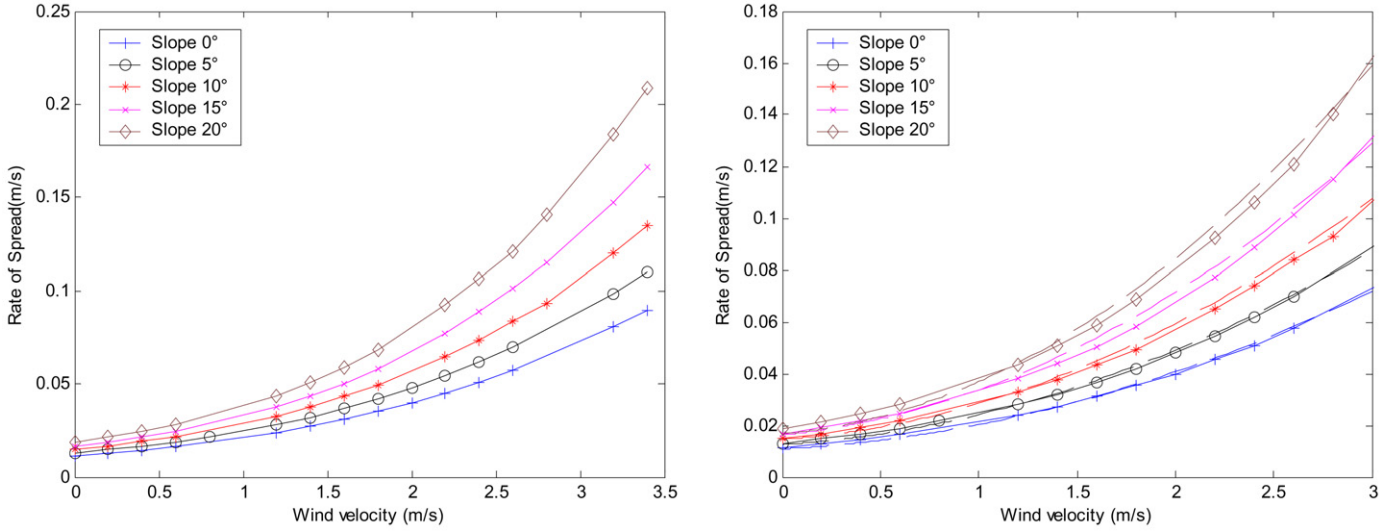

Fig. 4. Rate of spread versus slope and wind for the anisotropic propagation model with nonlocal radiative term.

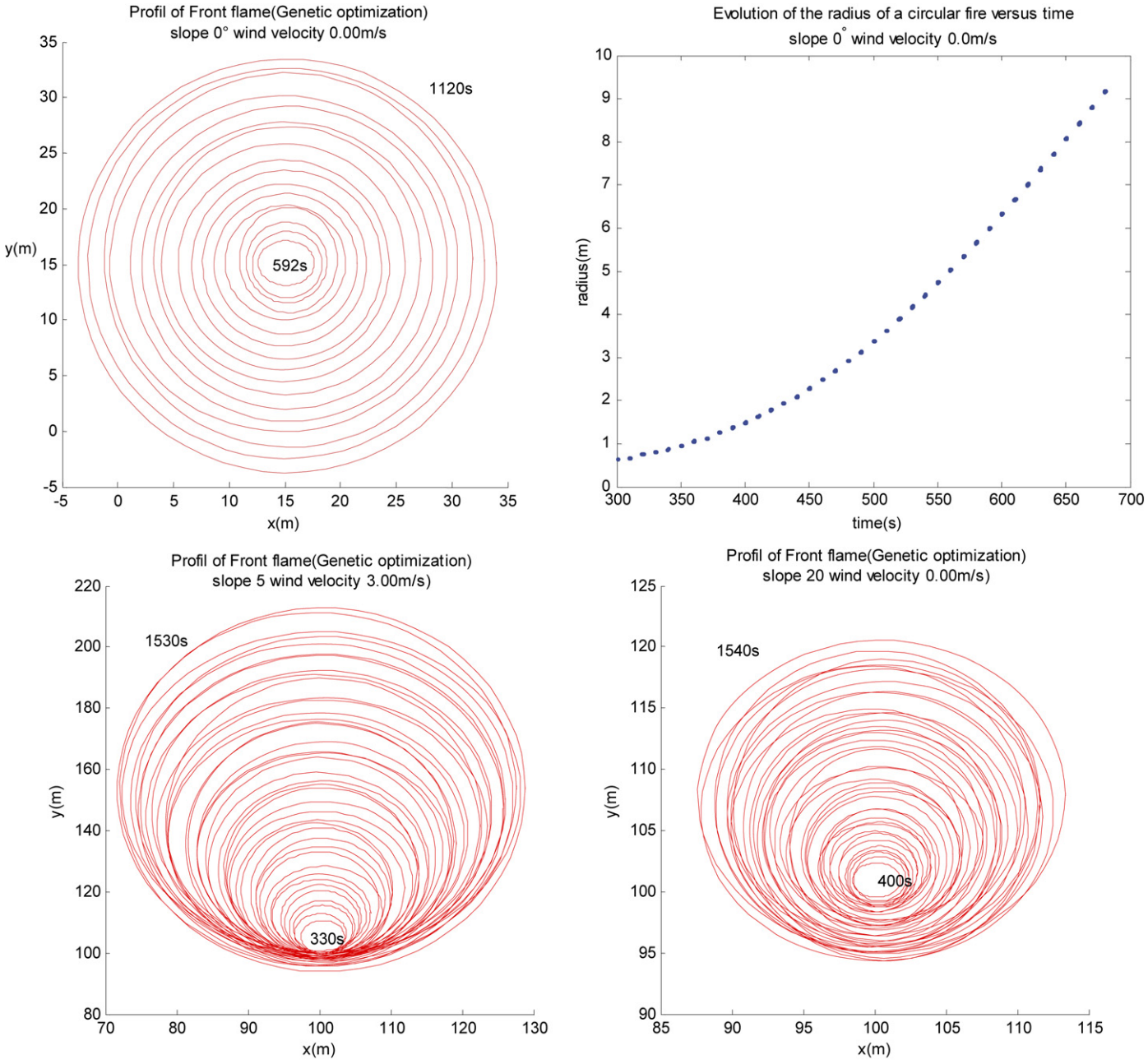

Fig. 5. Fire fronts at successive times for different slopes and winds. The ignition point is at $(x, y) = (100\text{ m}, 100\text{ m})$.

4.1. Straight line propagation

With the above physical values, one obtains the behaviour of Fig. 4 for the rate of spread, considering a straight line ignition.

This rate of spread is measured at the middle of the fire front when the stationary propagation is attained. The rate of spread values seem realistic, compared to experimental results given in Mendes-Lopes et al. [30] and Santoni et al. [31], for fires of small intensities on pine needles litters. Recall that, according to Eq. (16), the straight line rate of spread of the envelope method is given by the sum $f + g$ so that our model permits to determine this summation spread.

4.2. Point ignition

We have seen in the preceding Section 4.1 that the rate of spread given by the model can be compared favourably to experimental results for a straight fire front. In order to see if this anisotropic propagation model with nonlocal radiative term can contain the geometrical models presented in Section 2, it is necessary to show that a fire ignited at a point will develop an elliptical fire front.

On Figs. 5, we have plotted firstly the shape of the fire front with no slope and no wind, as foreseen the fire front is a circle. The transient time depends on the ignition process, which is supposed to approximate a Dirac δ function. On the right part of the figure, the radius of the circle is plotted versus time, one

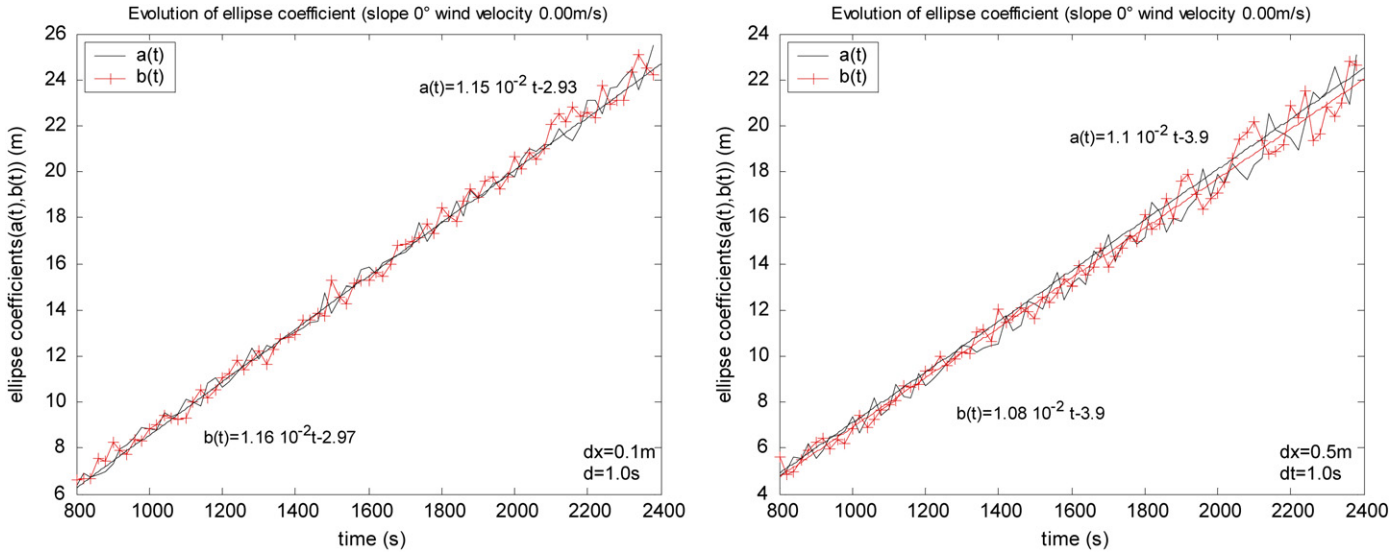

Fig. 6. Variations of the ellipse parameters with time and of the relative error. Slope 0°, wind 0 m s^{-1} mesh 0.1 m and 0.5 m.

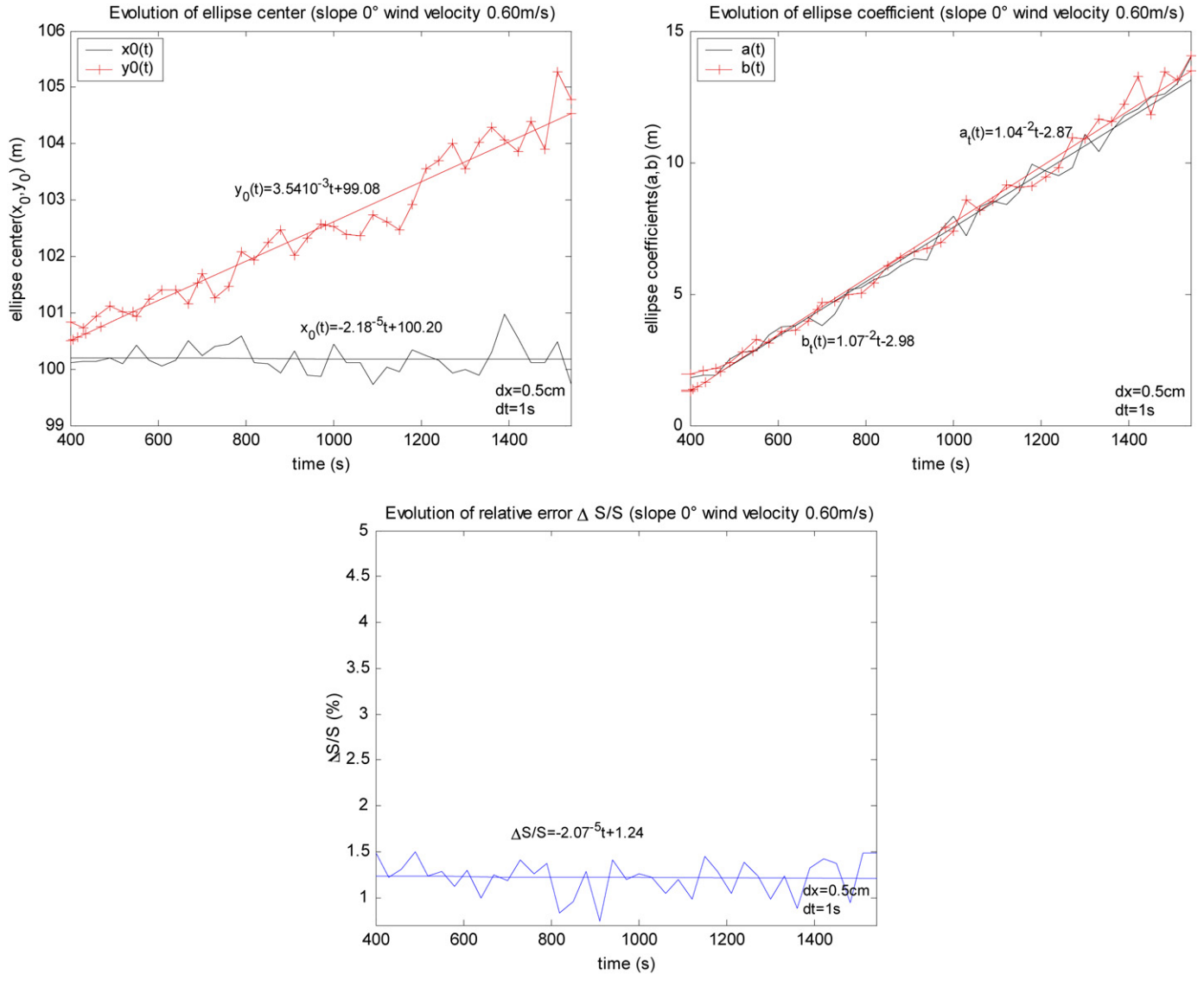

Fig. 7. Variations of the ellipse parameters with time and of the relative error. No slope, wind 0.60 m s^{-1}.

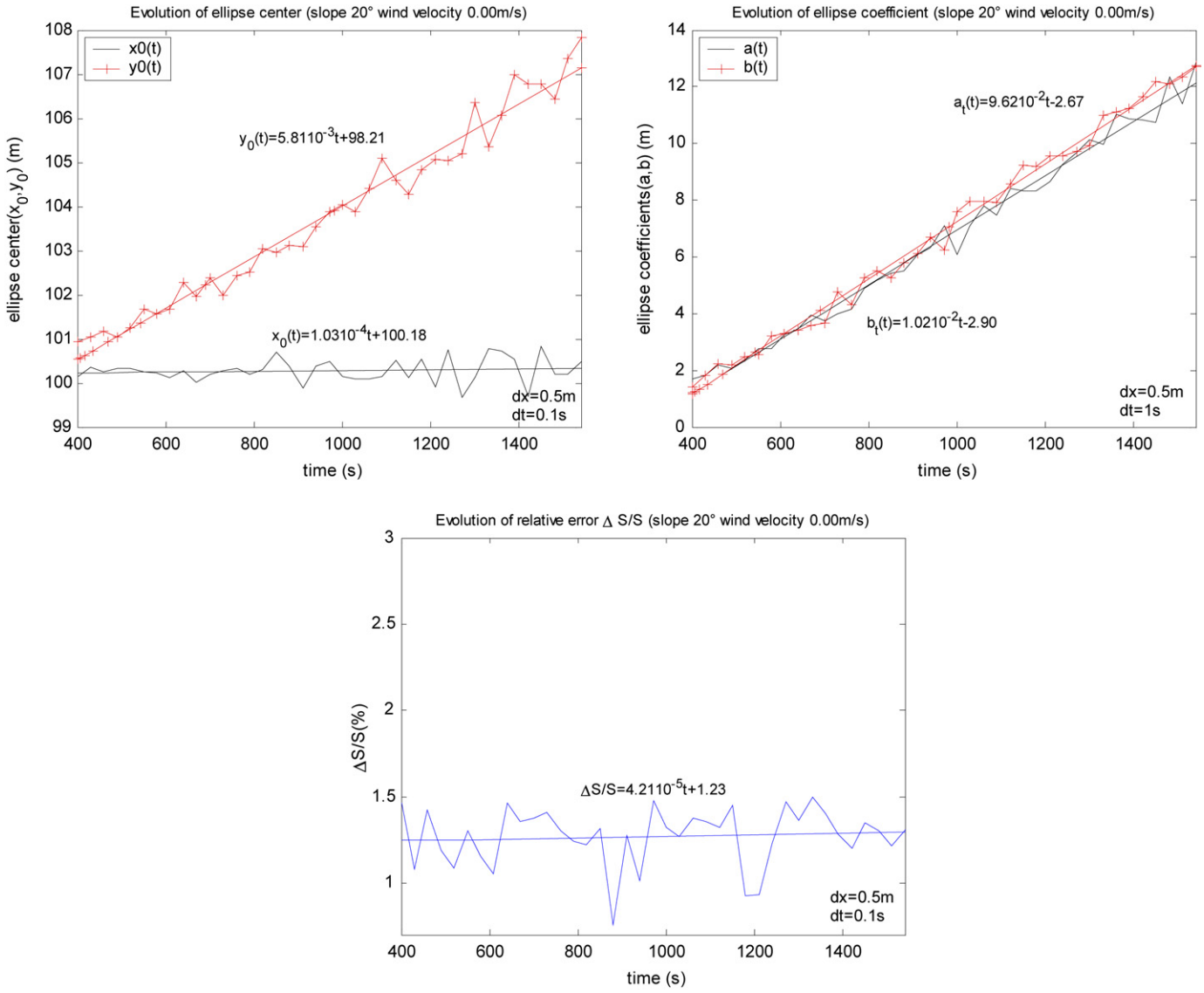

Fig. 8. Variations of the ellipse parameters with time and of the relative error. Slope 20°, no wind.

can see that the propagation is not immediately stationary and becomes stationary only after some times. On the other parts of the figures we have plotted the fire front curve at different time steps for two different slopes and winds that are directed along y axis. One can recognize that the fire line seems to be an ellipse. In order to compare, the fire lines have been fitted with the best possible ellipse:

$$\frac{(x-x_0)^2}{a^2}+\frac{(y-y_0)^2}{b^2}-1=0 \tag{56}$$

The best ellipse has been determined solving the minimum problem:

$$\min_{\substack{x_0,y_0\\a,b}} \Delta S \quad \text{with } \Delta S=\int_{R^2} |\chi_{\text{cal}}-\chi_{\text{ell}}|\,\mathrm{d}x\,\mathrm{d}y \tag{57}$$

In relation (53), χ_{cal}, χ_{ell} are the characteristic functions of respectively the burning and burnt zones, calculated by the model (45)–(55), and of the fitting ellipse so that ΔS is the area of the difference surface between the two zones. The optimisation problems are solved at each time steps using a genetic like algorithm. The fitting has been realised once the stationary state has been reached, that is why the curves have equation of the form $ut+v$ and do not go through the point $(0,0)$. The discontinuous aspect of the curve is due to the fact that at each time step not all the cells in the neighbour of the fire commute into the burning state exactly at the same time. This effect is diminished if the time step and mesh size are decreased.

In order to see the dependency of the results on mesh size, let us consider a mesh of 0.1 m, for a no wind and no slope case, see Fig. 6.

One can see that the results obtained are very close to the preceding ones, that is why computations have been made with the coarser mesh and time step.

Considering the relative error one can notice that the fire fronts are close to ellipses for all time steps and that the parameters x_0, y_0, a, and b vary linearly with time. This result is consistent with relations (8) of the envelope model. Indeed, by identifying Eqs. (8) and (11), we get $a=ht$, $b=ft$, $y_0=gt$,

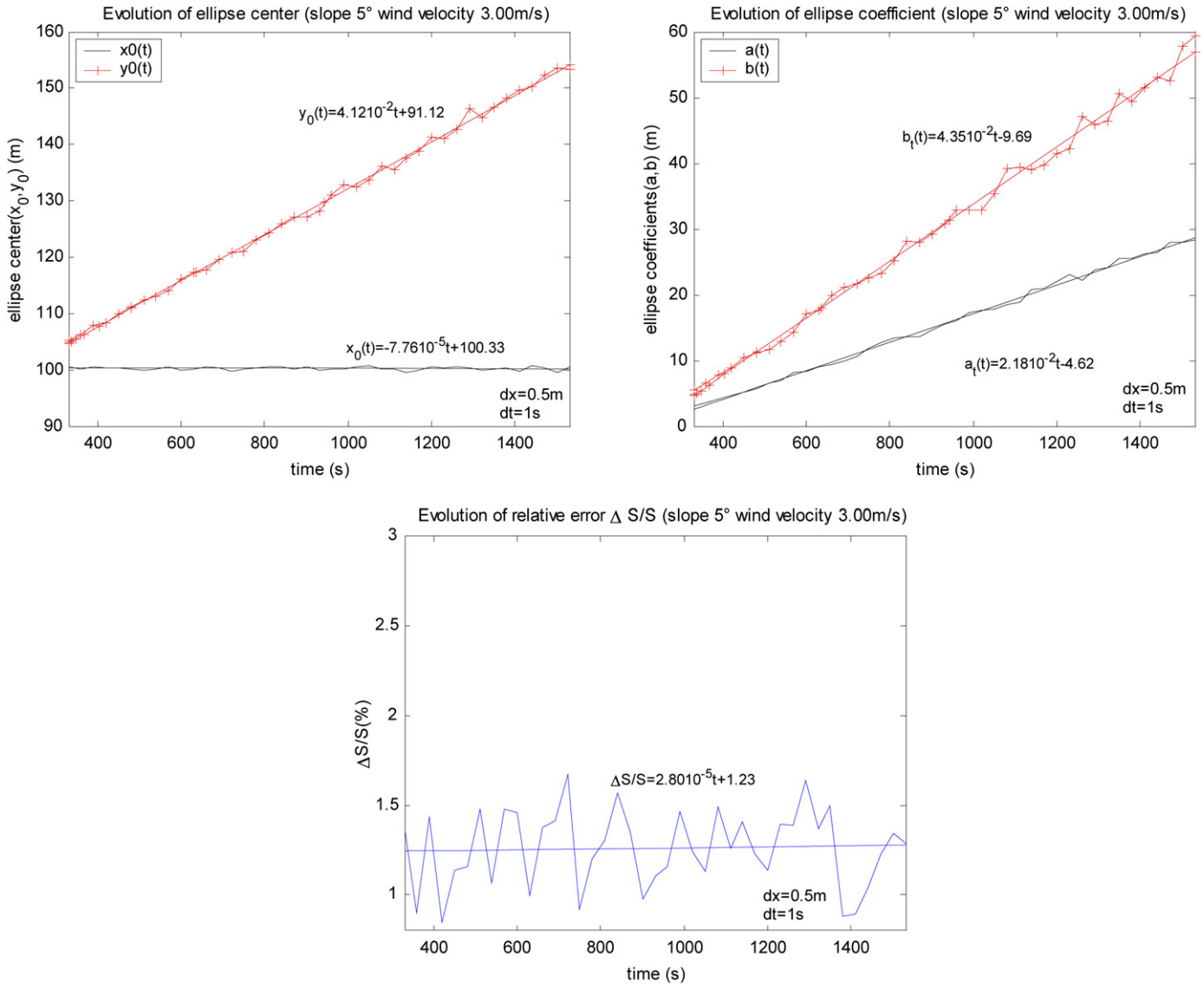

Fig. 9. Variations of the ellipse parameters with time and of the relative error. Slope 5°, wind 3 m s^{-1}.

and $x_0 = 0$. The measured rate of spread is exactly 0.049 which is the value of $f + g$. This equality has been verified for all computations.

Some results are given in the following Figs. 7 to 9. In order to determine the accuracy of fitting the fire front by an ellipse, the relative error $\frac{\Delta S}{S_{\text{cal}}}(t)$ has been plotted, S_{cal} being the surface of the calculated burning zone.

The first point to notice is that once the stationary state has been reached the variations of the coefficients are linear with time as expected, see relation (8). So that one can conclude that the anisotropic propagation model with nonlocal radiative term (NLRT) (45)–(55) presented here contains the envelope model. The second point is that although the relative error is an increasing function of time, the approximation of the fire front by an ellipse remains valid on a large range of time, this is due partly to the fact that the rate of spread is generally low (some centimetres/seconds to several tens centimetres/seconds). The third point is that the rates of spread obtained for the straight line ignition and the point ignition are consistent (results of Fig. 4).

The development of a numerical scheme for the model including diffusion is beyond the scope of this paper, because of the presence of several free boundaries and will be the scope of a different paper.

4.3. General curve line forest fire front

So far we have obtained that the anisotropic propagation with nonlocal radiative term model (NLRT) contains the envelope model and we have derived the corresponding values for the f, g, and h parameters from the point ignition simulation of the NLRT model. We will use these values for computing the envelope model and compare these results with the NLRT model for other ignition lines. It is now interesting to see cases when the present model and the envelope model give different results. The envelope model relies indeed on two implicit hypotheses:

- The propagation is stationary.

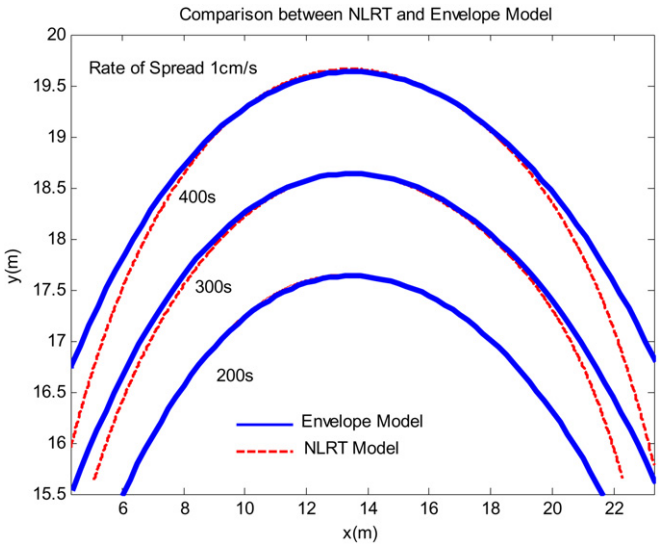

Fig. 10. Comparison of propagation for reaction model and envelope model for a sinus ignition line.

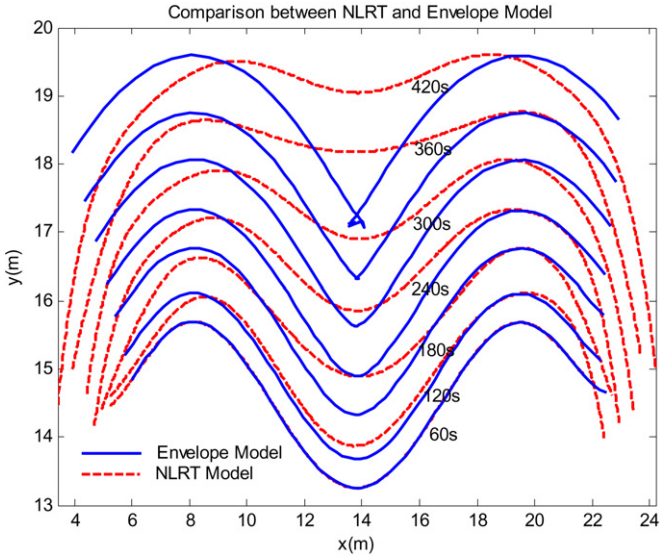

Fig. 11. Propagation with a two arches line ignition, no slope and no wind.

- The rate of spread depends only on local values of the parameters.

As we have noticed in the preceding paragraph the validity of the first hypothesis depends on the time needed for attaining the stationary propagation. After ignition, the rate of spread is an increasing function of time and reaches its maximum and stationary value after several hundred seconds for straight line ignition with parameters considered in the previous subsection 4.2. Therefore the envelope model will over estimate the propagation rate during the nonstationary phase. The second hypothesis can be questioned if for example different parts of the fire front can interact, due to the nonlocality of the radiative flux.

And in fact if different parts of the fire front interact then the process is not stationary.

In order to see this effect, let us ignite the fire with a sinus line and compare the propagation obtained by both models.

For the propagation in Fig. 10 there is no slope and no wind, so that $f = h$ and $g = 0$ for the envelope model. The parameters for the envelope model have been measured on a straight line ignition after 200 seconds of the simulation of the NLRT model. A sinus arch after the transient time has been propagated by both models and the fire lines are plotted on Fig. 10. Let us notice that the shape of the fire front is very similar in the centre (x between 8 and 18 m) but becomes different near the boundaries of the calculation domain. This is due to the fact that the rate of spread along the line obtained by the NLRT model is different from the envelope model because of the boundary effect, i.e., a combination of fire front curvature and nonlocality of the radiative flux. Points near the boundary receive less radiative flux than the points in the centre leading to a lower rate of spread. That tends to steepen the fire line.

The line ignition in Fig. 10 has only one concave arch. We can now consider a "complete" sinus with two concave arches and a convex one, and we do again the same experiment, the results are plotted in Fig. 11.

The flux in the reaction model is dispersed in the concave region therefore the rate of spread is decreased. It is concentrated in the convex region then the rate of spread is increased so that the central part of the curve tends to a line. On the other hand, the envelope model tends to steepen the slope of the front and develops a spurious caustic once the radius of fire front curvature in the convex region is too small. Here again we can notice that the discrepancy between both models appears after a relatively long time, this is again due to the low value of the rate of spread.

5. Conclusion

We have seen that Rothermel model is included in the envelope model and that the simplest extension of the envelope model is a reaction diffusion models. We have explored numerically the influence of the nonlocal radiative heat source on propagation. Although the diffusivity has not taken into account we have seen that the reaction model gives good results comparing the obtained rate of spread to experimental results and can be considered as an extension of the envelope model. Other simulations, not reported here, have shown that this result is insensitive to the type of considered flame model provide the flame model has a physically relevant dependency upon slope, wind and distance. The numerical solving of the model is somewhat complicated because of the presence of several free boundaries and the exposure of the numerical algorithm, with or without diffusivity will be considered in a separate paper. Indeed the question of the meaning and the value of the heat diffusivity has been partly addressed. It is mostly probable that diffusivity is not only the result of heat conduction at small scales, but that some "turbulent" diffusivity must be considered due to the average of heat transport processes at large scales.

The type of models presented here can be calibrated to give relevant results relatively to the rate of spread and of to the fire

front shape, the computation time is ten to one hundred faster than real time, depending of the power of the computer. Therefore it seems that they are good candidates for the physical modelling of small to moderate intensity forest fires at large scales and for real time applications. They can be used in situation where the envelope method cannot produce correct simulation of propagation. In some way, they represent one of the simplest extensions of Rothermel and envelope model. As for Rothermel model, they could be improved being calibrated with a large panel of experiments. For example, here, the characteristics of the flame (temperature, height, ...) have been considered as independent of the mass loss due to pyrolysis. It could be supposed that, as in pool fire, see Drysdale [32] for example, the law giving the flame parameters is function of the mass loss and this law could be obtained experimentally. Of course, parabolic reaction diffusion models, if they are confirmed as large scale forest fires propagation models, have a limited range of validity. The one presented have been obtained as a simplified part of the inner expansion of a porous medium combustion model. Most probably the convective heating is not well modelled and will be improved in the future.

Appendix A

Let us now derive relation (52).

We will assume that the flame and the vegetation are grey medium with constant absorption coefficients K_f, K_v.

Then if the temperature T_f of the flame is constant the integration of the radiative transfer equation gives for the intensity

$$i(s) = \frac{BT_f^4}{\pi}\left(1 - \mathrm{e}^{-K_f(s_2-s_1)}\right)\mathrm{e}^{-K_v(s-s_3)} + K_v \int_{s_3}^{s} i_b(\bar{s})\mathrm{e}^{-K_v(s-\bar{s})}\,\mathrm{d}\bar{s} \tag{A.1}$$

with $B = n^2\sigma$, σ being the Boltzmann constant and n the optical indice of the medium.

If the flame is assumed thin $(1 - \mathrm{e}^{-K_f(s_2-s_1)}) \approx K_f(s_2 - s_1) = K_f \int_{s_1}^{s_2} \mathrm{d}\bar{s}$ and the preceding relation becomes:

$$i(s) = K_f \frac{BT_f^4}{\pi}\mathrm{e}^{-K_v(s-s_3)} \int_{s_1}^{s_2} \mathrm{d}\bar{s} + K_v \int_{s_3}^{s} i_b(\bar{s})\mathrm{e}^{-K_v(s-\bar{s})}\,\mathrm{d}\bar{s} \tag{A.2}$$

Then the radiative flux density received by a surface with normal $\mathbf{n}_i$ is:

$$\mathbf{q}_r(\mathbf{M})\cdot\mathbf{n}_i = K_f \frac{BT_f^4}{\pi}\int_{\Omega_f} \frac{\mathrm{e}^{-K_v\mathbf{aM}}}{\mathbf{PM}^2}\mathbf{u}\cdot\mathbf{n}_i\,\mathrm{d}\Omega(\mathbf{P}) + K_v \frac{BT_v^4}{\pi}\int_{\Omega_v} \frac{\mathrm{e}^{-K_v\mathbf{AM}}}{\mathbf{AM}^2}\mathbf{u}\cdot\mathbf{n}_i\,\mathrm{d}\Omega(\mathbf{P}) \tag{A.3}$$

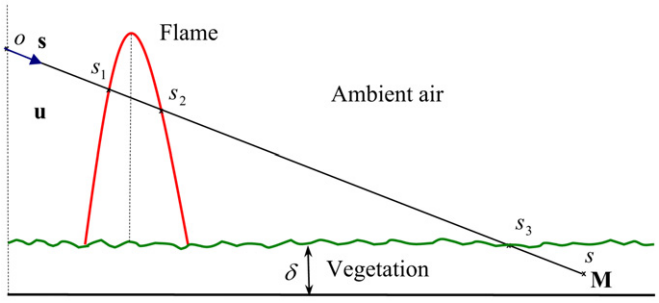

Fig. A.1.

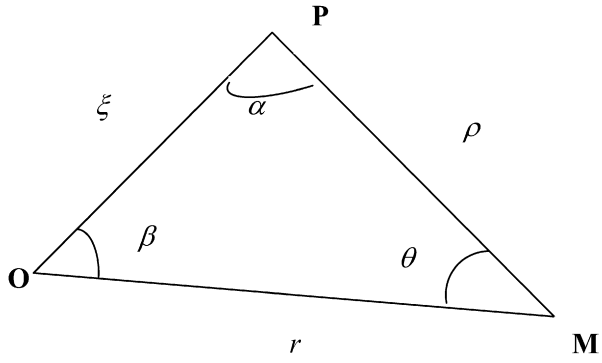

Fig. A.2.

Where Ω_f is the domain occupied by the flame and Ω_v is the domain occupied by the vegetation. In the limit $\delta \to 0$ the right-hand side of (A.2) reduces to:

$$\mathbf{q}_r(\mathbf{M})\cdot\mathbf{n} = K_f \frac{BT_f^4}{\pi}\int_{\Omega_f} \frac{1}{\mathbf{PM}^2}\mathbf{u}\cdot\mathbf{n}\,\mathrm{d}\Omega(\mathbf{P}) \tag{A.4}$$

This triple integral can be reduced to a double integral. Let us consider that each element of flames is directed by a unit vector $\mathbf{F}$, $\mathbf{n}$ is the unit vector normal to the plane Π_v which is the top of vegetation at the receiving point M. If we consider an absolute co-ordinate system $(O, \mathbf{e}_1, \mathbf{e}_2, \mathbf{e}_3)$ (not drawn on figure above), we define the following angles:

$$(\mathbf{e}_3, \mathbf{F}) = \alpha_f, \quad (\mathbf{F}, \mathbf{OM}) = \beta \tag{A.5}$$

The emitting point on the flame is the point $\mathbf{P}$, the point $\mathbf{O}$ is the flame foot, and we consider the radial co-ordinate r, such that

$$\|\mathbf{PM}\| = \rho, \quad \mathbf{OP} = \xi\mathbf{F}, \quad \text{and} \quad \mathbf{OM} = r\mathbf{w}.$$

Then $\mathbf{PM} = \mathbf{OM} - \mathbf{OP} = r\mathbf{w} - \xi\mathbf{F}$, and $\mathbf{u}\cdot\mathbf{n} = \frac{1}{\rho}(r\mathbf{w}\cdot\mathbf{n} - \xi\mathbf{F}\cdot\mathbf{n})$.

In the triple integral of the right-hand side of (A.3) we integrate first along the flame, with the previous notations, we obtain:

$$M_r = -\mathbf{q}_r(\mathbf{M})\cdot\mathbf{n} = -K_f \frac{BT_f^4}{\pi}\int_{S_f} \frac{\mathrm{d}x\,\mathrm{d}y}{\cos\alpha_f}\int_0^{l_f} \frac{1}{\rho^3}(r\mathbf{w}\cdot\mathbf{n} - \xi\mathbf{F}\cdot\mathbf{n})\,\mathrm{d}\xi \tag{A.6}$$

In (A.6) S_f is the burning surface and l_f the local flame length. The simple integrals $\int_0^{l_f} \frac{\xi}{\rho^3}\,\mathrm{d}\xi$ and $\int_0^{l_f} \frac{r}{\rho^3}\,\mathrm{d}\xi$ can be evaluated.

Let us consider the triangle OPM and the different angles in this triangle cf. Fig. A.2.

Then we have the following relations:

$$\frac{\rho}{\sin\beta} = \frac{r}{\sin\alpha} = \frac{\xi}{\sin\theta} \quad \text{with } \alpha+\beta+\theta=\pi. \tag{A.7}$$

Then θ can be used as parameter. The derivation of (A.6) gives:

$$\mathrm{d}\xi = r\frac{\sin\beta}{\sin^2(\beta+\theta)}\,\mathrm{d}\theta = r\frac{\sin\beta}{\sin^2\alpha}\,\mathrm{d}\theta \tag{A.8}$$

Then:

$$I_1 = \int_0^{l_f} \frac{r}{\rho^3}\,\mathrm{d}\xi = \frac{1}{r\sin^2\beta}\int_0^{\theta_{fm}} \sin(\beta+\theta)\,\mathrm{d}\theta$$
$$= \frac{1}{r\sin^2\beta}\big(\cos\beta - \cos(\beta+\theta_{f_m})\big) \tag{A.9}$$

$$I_2 = \int_0^{l_f} \frac{\xi}{\rho^3}\,\mathrm{d}\xi$$
$$= \frac{1}{r\sin^2\beta}\int_0^{\theta_{fm}} \sin\theta\,\mathrm{d}\theta = \frac{1}{r\sin^2\beta}(1-\cos\theta_{f_m}) \tag{A.10}$$

Once (A.8) and (A.9) are put in the integral on obtains:

$$M_r = K_f\frac{BT_f^4}{\pi} \times \int_{S_f} \frac{(\mathbf{F}(1-\cos\theta_{f_m}) - \mathbf{w}(\cos\beta-\cos(\beta+\theta_{f_m}))\cdot\mathbf{n}}{r\sin^2\beta}\,\mathrm{d}x\,\mathrm{d}y \tag{A.11}$$

With θ_{f_m} and β solutions to the equations:

$$\cos\beta = \mathbf{F}\cdot\frac{\mathbf{OM}}{r}, \qquad \cot\theta_{f_m} = \frac{r}{l_f\sin\beta} - \cot\beta \tag{A.12}$$

Acknowledgements

The support of the European community, research contract "SPREAD" n° EVG1-CT-2001-00043 and of the French Ministry of Research contract "PAREFEU" are greatly acknowledged.

References

[1] O. Séro-Guillaume, J. Margerit, Int. J. Heat Mass Transfer 45 (2002) 1705–1722.
[2] C. Di Blasi, Prog. Energy Combust. Sci. 19 (1993) 71–104.
[3] A.M. Grishin, Mathematical Modeling of Forest Fires and New Methods of Fighting Them, Tomsk State University, Tomsk, Russia, 1997, 390 p.
[4] R.R. Linn, Transport model for prediction of wildland fire behaviour, Los Alamos National Laboratory, Scientific Report, LA13334-T, 1997.
[5] F.A. Albini, Combust. Sci. Technol. 42 (1985) 229–258.
[6] F.A. Albini, Combust. Sci. Technol. 45 (1985) 101–113.
[7] B. Porterie, D. Morvan, J.C. Loraud, M. Larini, Phys. Fluids 12 (7) (2000) 1762–1782.
[8] A.J. Majda, P.E. Souganidis, Nonlinearity 7 (1994) 1–30.
[9] P. Clavin, F.A. Williams, J. Fluid Mech. 90 (1979) 589–604.
[10] R.O. Weber, Combust. Flame 78 (1989) 398–408.
[11] R.O. Weber, Int. J. Wildland Fire 1 (4) (1991) 245–248.
[12] G. Albinet, G. Searby, D. Stauffer, J. Physique 47 (1986) 1–7.
[13] T. Beer, Combust. Sci. Technol. 72 (4–6) (1990) 297–304.
[14] J.R. Weimar, J.P. Boon, Phys. Rev. E 49 (2) (1994) 1749–1752.
[15] Zekri, B. Porterie, J.P. Clerc, J.C. Loraud, Phys. Rev. E 71 (2005) 046121, 1–15.
[16] R.C. Rothermel, A mathematical model for predicting fire spread in wildland fuels, USDA Forest Service, 1972, Research paper INT-115, Ogden, Utah, USA, 40 p.
[17] G.B. Peet, Aus. Forestry 31 (1967) 121–127.
[18] J.C. Drouet, Etude théorique de la lutte contre les feux de forêts, Thèse de Doctorat des Sciences, Université de Provence, 6/10/1972.
[19] D.H. Anderson, E.A. Catchpole, N.J. De Mestre, T. Parkes, J. Austral. Math. Soc. (Series B) 13 (1982) 452–466.
[20] E.A. Catchpole, M.E. Alexander, A.M. Gill, Can. J. Forest Res. 12 (1992) 968–972.
[21] G.D. Richards, Int. J. Numer. Meth. Eng. 30 (1990) 1163–1179.
[22] S. Sieniutycz, H. Farkas, Chem. Engrg. Sci. 52 (17) (1997) 2927–2945.
[23] P. Enders, Eur. J. Phys. 17 (1996) 226–235.
[24] R. Courant, D. Hilbert, Methods of Mathematical Physics, vols. I, II, Interscience, New York–London, 1962.
[25] M.A. Finney, Modelling the spread and behaviour of prescribed natural fires, in: D.X. Viegas (Ed.), Proc. 12th Conf. Fire and Forest Meteorology, 1994, pp. 138–143.
[26] C. Moyne, S. Didierjean, H.P. Amaral Souto, O.T. Da Silveira, Int. J. Heat Mass Transfer 43 (2000) 3853–3867.
[27] A. Fannjiang, G. Papanicolaou, SIAM J. Appl. Math. 54 (2) (1994) 333–408.
[28] J. Margerit, O. Séro-Guillaume, Int. J. Heat Mass Transfer 45 (2002) 1723–1737.
[29] K. Chetehouna, M. Er-Riani, O. Séro-Guillaume, Numer. Heat Transfer, Part A 46 (8) (2004) 765–784.
[30] J.M.C. Mendes-Lopes, J.M.P. Amaral, in: D.X. Viegas (Ed.), 3rd International Conference on Forest Fire Research, 1, 1998, pp. 497–511.
[31] P.A. Santoni, J.H. Balbi, J.L. Dupuy, Int. J. Wildland Fire 9 (4) (1999) 285–292.
[32] D. Drysdale, An Introduction to Fire Dynamics, second ed., John Willey, 2003.